JOURNAL OF AIRCRAFT
Vol. 39, No. 4, July–August 2002

Helicopter Vibration Reduction Using Discrete Controllable-Stiffness Devices at the Rotor Hub

Farhan Gandhi* and Phuriwat Anusonti-Inthra†
Pennsylvania State University, University Park, Pennsylvania 16802

The present study demonstrates that optimal multi-cyclic stiffness variations of discrete controllable stiffness devices in the rotor blade root region can reduce the 4/rev vibratory hub loads of a four-bladed hingeless rotor helicopter. The controllable stiffness devices (flap, lag, and torsion devices) are modeled as discrete springs whose stiffness coefficients can be varied, and a gradient-based optimization scheme is used to determine optimal multi-cyclic device stiffness variations that minimize a composite index comprising of all six components of vibratory hub loads. Multi-cyclic stiffness variations of the flap and lag devices are most influential, and when optimal 2/rev and 3/rev stiffness variations of these devices were used in combination the vibratory hub drag force was practically eliminated and the vibratory hub side force was reduced by 55%. No significant detrimental effects were observed on the first through the fifth harmonics of the vibratory blade root loads. Multi-cyclic (3/rev and 4/rev) stiffness variations of the torsion device produced only small reductions in the 4/rev hub vertical force. Multi-cyclic stiffness variations of the flap and lag devices were seen to be effective in reducing hub vibration even when there were changes in fundamental rotor properties such as the flap, lag, and torsion stiffness of the root (flexure) element, and the cruise speed.

I. Introduction

IN forward flight helicopters can experience severe vibration caused by the rotor blades operating in a periodic aerodynamic environment. These vibrations result in significant crew and passenger discomfort, increased component fatigue and maintenance requirements, and reduced effectiveness of sensitive equipment and weapon systems for military helicopters. Accordingly, considerable effort has been devoted over the past several decades to examine passive design and active control strategies for helicopter vibration reduction (for example, see Refs. 1–10).

Common techniques for passive vibration reduction include use of vibration absorbers, isolators, and structural and aerodynamic design optimization of the rotor blades. Although these concepts can produce some vibration reduction, they generally involve a significant weight penalty and are tuned to a specific flight/operating condition (inability to adapt to changes in conditions). Active vibration reduction strategies have also been examined extensively—including higher harmonic pitch control or HHC, individual blade control or IBC (through root pitch actuation, trailing edge flap actuation, active blade twist, etc.), and active control of structural response or ACSR. HHC and IBC involve generating unsteady higher harmonic aerodynamic loads that cancel the original vibratory loads at the source. Although these methods can be effective, they usually involve high power requirements, added weight and complexity, and high pitch-link loads. Further, IBC requires use of slip rings capable of transferring enough power to the actuators in the rotating frame. ACSR uses actuators carefully located in the airframe to actively cancel the incoming N/rev vibratory loads from the rotor. Although this method can locally reduce airframe vibration, the high vibration levels and dynamic stresses experienced by the rotor blades remain unaltered.

Recently a new semi-active approach was proposed for helicopter vibration reduction,[11,12] involving cyclic variation of the effective flap, lag, and torsion stiffness of the blade root region. It was shown that by introducing small-to-moderate amplitude stiffness variations at harmonics of the rotor speed considerable reduction in vibratory hub loads was possible. A semi-active approach differs from purely active approaches to rotor control (HHC and IBC) in that large aerodynamic forces do not have to be directly overcome in every cycle (a requirement with pure active approaches involving twisting of the blade, changing of the blade pitch, or deflection of a trailing-edge flap). Consequently, power requirements for semi-active control schemes tend to be substantially smaller for comparable performance, and such strategies have already been explored for vibration suppression applications such as controlling the structural response caused by earthquakes (for example, see Refs. 13–16) and in the design of suspensions in the automobile industry (for example, see Refs. 17–20). An additional advantage of semi-active control is that unlike pure active control little energy is being pumped into the controlled system, so that there is little or no potential for instability. Although both semi-active as well as pure active rotor control favorably modify the higher harmonic rotor blade response in reducing vibration, a semi-active approach achieves this by modulating the system properties, whereas pure active approaches generate forces and moments on the blade. In practice, stiffness variations of the rotor blade root region could be achieved by introducing discrete devices such as controllable orifice devices[21] or controllable electrorheological or magnetorheological fluid-based devices in the blade root region.[22,23] In a previous study the authors clearly established the sensitivity of hub vibrations to individual cyclic variations in the flap, lag, and torsion stiffness of the blade root region and explained the underlying physical mechanisms by which vibration reductions were achieved.[11] This was followed by the use of formal optimization methods to determine the combined multi-cyclic stiffness variations in flap, lag, and torsion that minimized a composite vibration index comprising of all components of N/rev vibratory hub loads.[12] However, in both of these studies the flexural or torsional stiffness of the entire root element (Rotor blade is discretized along the span using finite element method.) was cyclically varied, and the practical implementation of stiffness variations of the blade root region through discrete controllable-stiffness devices was not examined.

Received 19 January 2001; presented as Paper 2001-1438 at the AIAA/ASME/ASCE/AHS/ASC 42nd Structures, Structural Dynamics, and Materials Conference, 16–19 April 2001; revision received 6 March 2002; accepted for publication 22 March 2002.

*Associate Professor, Rotorcraft Center of Excellence, Department of Aerospace Engineering, 229 Hammond Building; fgandhi@psu.edu. Member AIAA.

†Graduate Research Assistant, Rotorcraft Center of Excellence, Department of Aerospace Engineering, 229 Hammond Building.

II. Focus of the Present Study

The present study examines the effectiveness of semi-active discrete controllable-stiffness devices introduced in the blade root region in reducing the 4/rev hub vibrations of a light BO-105 type four-bladed hingeless rotor helicopter. The controllable stiffness devices are modeled as discrete springs whose spring coefficients can be cyclically varied and can thereby produce cyclic variations in effective flap stiffness, lag stiffness, and torsion stiffness of the blade. Considering each device individually at first, a gradient-based approach is used to determine optimal multi-cyclic stiffness variations that minimize a composite vibration index (comprising of all six components of vibratory hub loads), and the effect of these optimal inputs on the hub vibrations are examined. Next, reductions in hub vibratory loads are examined when the devices are used in combination, and the influence of the optimal multi-cyclic stiffness variations on the vibratory blade root loads is examined as well. The effectiveness of this semi-active control scheme in reducing helicopter hub vibration is evaluated for variations in system parameters such as the blade root (flexure) element flap, lag, and torsion stiffness, as well as variations in cruise speed.

III. Analysis Method

To evaluate the effectiveness of optimal multi-cyclic stiffness variations of discrete controllable-stiffness devices introduced in the blade root region in reducing helicopter hub vibration, a comprehensive rotorcraft aeroelastic analysis based on the UMARC formulation[24] is used. A BO-105 type four-bladed hingeless rotor helicopter is simulated, with the blades assumed to undergo elastic flap and lag bending and elastic torsion deformations. The sectional aerodynamic loads are calculated using blade element theory, with the inflow calculated using a free-wake methodology.[25,26] In the analysis the blades are discretized along the span using the finite element method, and the discretized blade equations of motion are transformed to modal space to reduce computational cost. Blade periodic response in forward flight is calculated using the temporal finite element method. Evaluation of blade response and vehicle orientation and controls is carried out iteratively in a coupled response-trim calculation procedure. Such a coupled solution procedure is required because the blade response influences the steady rotor hub forces and moments, which appear in the vehicle equilibrium equations and impact the vehicle orientation and control settings. The new orientation and controls, in turn, affect the blade response. The converged solution yields the vehicle orientation and controls, blade periodic response, as well as the vibratory blade root loads and hub loads.

The root stiffness variations are implemented through discrete controllable stiffness devices in the root region of the blade (see schematic sketch, Fig. 1a). These devices are mathematically represented by the controllable springs K_w, K_v, and K_ϕ (as shown in Figs. 1b–1d). For the flap and lag controllable stiffness devices configuration and attachment geometry are shown in Fig. 2. While one end of the device is attached to the rotor hub, the other end is attached to the rotor blade at a finite element node so that the motion of that point (required to determine the device forces) is directly available, and semi-active forces and moments exerted on the blade are easily accounted for. The semi-active force generated depends on both the instantaneous stiffness of the devices as well as the blade motion at the attachment point, which governs the relative displacement of the controllable springs. Figure 3a shows the deformation of the flap device caused by flap bending motion of the blade. From the geometry and kinematics it can be shown that the flap spring deformation caused by flap displacement w and slope w' at the attachment point is given by

$$\Delta L_w = -w \sin\alpha_w - e_w w' \cos\alpha_w \tag{1}$$

Similarly, if v and v' are the lag-bending displacement and slope at the point the controllable lag spring is attached to the blade the deformation of the lag spring can be shown to be

$$\Delta L_v = -v \sin\alpha_v - e_v v' \cos\alpha_v \tag{2}$$

In Eqs. (1) and (2), α_w and α_v are the attachment angles of the flap and lag devices, and e_w and e_v are the attachment offsets (as seen in Figs. 2). The semi-active flap device force F_w^K and lag device force F_v^K are then expressed as

$$F_w^K = -K_w \Delta L_w, \qquad F_v^K = -K_v \Delta L_v \tag{3}$$

with K_w and K_v representing the instantaneous stiffness of the controllable flap and lag devices, respectively. The devices exert both forces and bending moments on the blade at the point of attachment in the flap and lag directions (see Fig. 3b for the force and moment on the blade caused by the flap device). The resulting loads

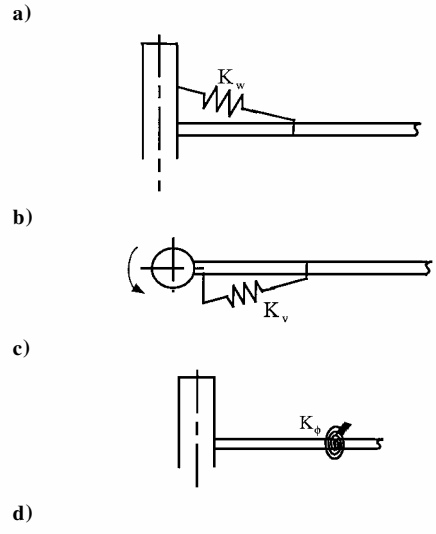

Fig. 1 Discrete controllable stiffness devices at the rotor hub a) Schematic diagram of discrete controllable stiffness devices and their mathematical idealization in b) flap, c) lead-lag, and d) torsion directions.

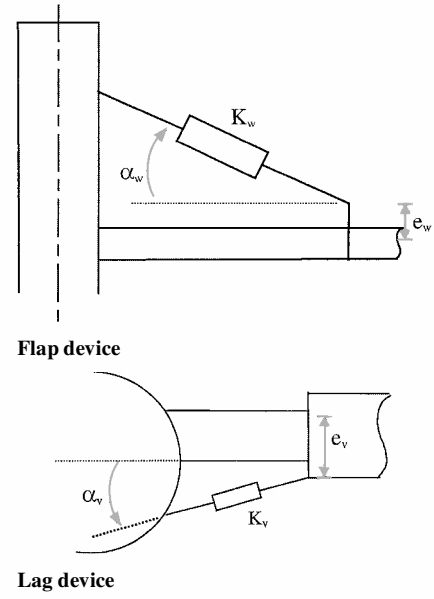

Fig. 2 Configuration and attachment geometry of controllable stiffness devices.

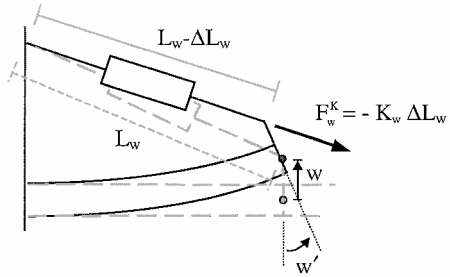

Fig. 3a Deformation of the flap device caused by blade bending.

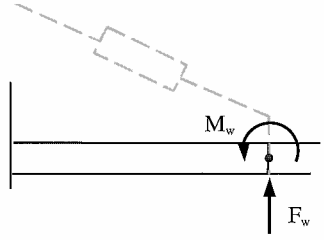

Fig. 3b Loads exerted on the blade at attachment point by the flap device.

at the blade finite element nodes (flap-bending shear force F_w and moment M_w, lag-bending shear force F_v and moment M_v) can be represented as

$$\begin{Bmatrix} F_w \\ M_w \end{Bmatrix} = -K_w \begin{bmatrix} \sin^2\alpha_w & e_w \sin\alpha_w \cos\alpha_w \\ e_w \sin\alpha_w \cos\alpha_w & (e_w \cos\alpha_w)^2 \end{bmatrix} \begin{Bmatrix} w \\ w' \end{Bmatrix} \tag{4a}$$

$$\begin{Bmatrix} F_v \\ M_v \end{Bmatrix} = -K_v \begin{bmatrix} \sin^2\alpha_v & e_v \sin\alpha_v \cos\alpha_v \\ e_v \sin\alpha_v \cos\alpha_v & (e_v \cos\alpha_v)^2 \end{bmatrix} \begin{Bmatrix} v \\ v' \end{Bmatrix} \tag{4b}$$

Further, the torsion moment acting on the blade at the attachment point of the torsion stiffness device is expressed as

$$M_\phi = -K_\phi \phi \tag{4c}$$

Because the blade loads in Eqs. (4a–4c) are dependent on the blade response at the attachment point (w, w', v, v', and ϕ), they will result in a modification of the blade stiffness matrices.

Cyclic variations in flap, lag, and torsion spring stiffness are then represented as follows:

$$K_w = K_w(\psi) = \bar{K}_w + \sum_{n=1}^{N} \left[\Delta K_w^n \sin\left(n\psi + \phi_n^w\right)\right] \tag{5a}$$

$$K_v = K_v(\psi) = \bar{K}_v + \sum_{n=1}^{N} \left[\Delta K_v^n \sin\left(n\psi + \phi_n^v\right)\right] \tag{5b}$$

$$K_\phi = K_\phi(\psi) = \bar{K}_\phi + \sum_{n=1}^{N} \left[\Delta K_\phi^n \sin\left(n\psi + \phi_n^\phi\right)\right] \tag{5c}$$

In the preceding equations n represents the frequency of the stiffness variations ($n = 2$ implies 2/rev variations, $n = 3$ implies 3/rev variations, etc.), and ϕ_n represents the phase angle corresponding to stiffness variation at n/rev. For discussions in this paper, the amplitudes of flap, lag, and torsion spring stiffness variations ΔK_w, ΔK_v, and ΔK_ϕ are expressed as percentages of their baseline values ($\bar{K}_w$, $\bar{K}_v$, and $\bar{K}_\phi$, respectively). From a practical standpoint the maximum stiffness variations achievable by the discrete devices will be bounded and cannot exceed a prescribed percentage of the baseline stiffness ($\bar{K}_w$, $\bar{K}_v$, or $\bar{K}_\phi$). Equations (5) can be written in a compact form as

$$K(\psi) = \bar{K} + \sum_{n=1}^{N} \left[\Delta K^n \sin(n\psi + \phi_n)\right] \tag{6}$$

The coupled blade flap-lag-torsion equations of motion can then be written symbolically as

$$m\overset{**}{q} + c\overset{*}{q} + \{k + \Delta k(\psi)\}q = F^{NL}$$

or

$$m\overset{**}{q} + c\overset{*}{q} + kq = F^{NL} - \Delta k(\psi)q \tag{7}$$

where $\Delta k(\psi)$ represents the component of the stiffness matrix with periodically varying terms as a result of the controllable stiffness devices and F^{NL} includes all of the motion independent forces as well as nonlinear elastic, inertial, and aerodynamic contributions. Clearly, the $\Delta k(\psi)q$ term (from device stiffness variations) can be regarded as an unsteady loading that, in essence, can be used to modify the blade responses as desired. Traditional HHC or IBC produce desired responses for vibration reduction by generating unsteady aerodynamic forces at 3/rev, 4/rev, and 5/rev (for a four-bladed rotor). In the present semi-active concept because the blade periodic response q itself contains harmonics of rotor frequency, lower harmonic variations of device stiffness $\Delta K(\psi)$ are also able to generate unsteady loads $\Delta k(\psi)q$ at 3/rev, 4/rev, and 5/rev for a four-bladed rotor. References 11 and 12 demonstrated that 2/rev and 3/rev blade root flap and lag stiffness variations and 3/rev and 4/rev blade root torsion stiffness variations were particularly effective in reducing 4/rev hub vibrations.

To determine the optimal spring stiffness variation $\Delta K(\psi)$, a frequency-domain approach is used, similar to that employed in previous active vibration reduction studies.[27] Instead of the active control inputs (blade pitch or trailing-edge flap inputs), it is assumed that the harmonics of spring stiffness variations ΔK relate to the helicopter hub vibrations z (z comprises all components of vibratory hub loads, $z = \lfloor F_x^{4p} F_y^{4p} F_z^{4p} M_x^{4p} M_y^{4p} M_z^{4p} \rfloor^T$), through a transfer function T as follows:

$$z = z_0 + T\Delta K \tag{8}$$

where z_0 represents the baseline 4/rev hub vibration and z represents 4/rev hub vibration in the presence of variation in spring stiffness ΔK.

$$\Delta K = \Big[\underbrace{\Delta K_w^{2c} \quad \Delta K_w^{2s} \quad \Delta K_w^{3c} \quad \Delta K_w^{3s}}_{\text{2,3/rev stiffness variations of the flap device}} \underbrace{\Delta K_v^{2c} \quad \Delta K_v^{2s} \quad \Delta K_v^{3c} \quad \Delta K_v^{3s}}_{\text{2,3/rev stiffness variations of the lag device}}$$

$$\times \underbrace{\Delta K_\phi^{3c} \quad \Delta K_\phi^{3s} \quad \Delta K_\phi^{4c} \quad \Delta K_\phi^{4s}}_{\text{3,4/rev stiffness variations of the torsion device}} \Big]^T \tag{9}$$

The transfer matrix T is numerically calculated by perturbation of individual stiffness components about the baseline configuration.

The control algorithm, adapted from Ref. 27, is based on the minimization of a composite quadratic objective function J defined as

$$J = J_z + J_k = z^T W_z z + \Delta K^T W_k \Delta K \tag{10}$$

where W_z represents the weighting on output vibration ($W_z = \frac{1}{6}\lfloor z_0^T z_0 \rfloor^{-1}$) and W_k represents the penalty weighting on input (assumed to be the identity matrix unless otherwise stated). Gradient-based methods are used to minimize J and determine the optimal input (stiffness variations). An optimal solution can be found by substituting Eq. (8) into Eq. (10) and setting $\partial J/\partial \Delta K = 0$. The resulting optimal stiffness variation input is

$$\Delta K = -(T^T W_z T + W_k)^{-1} T^T W_z z_0 \tag{11}$$

In the optimization studies of the following sections, $J_z = z^T W_z z$ (which is a measure of the vibration level) is used as a composite vibration performance index, with smaller values of J_z indicating more vibration reduction as a result of cyclic stiffness variations ($J_z = 100$ for the baseline, with no cyclic stiffness variations).

IV. Results and Discussion

A. Baseline Configuration

Effectiveness of discrete controllable stiffness devices in reducing rotor hub vibrations is examined on a BO-105 type four-bladed hingeless rotor helicopter whose properties are given in Table 1. In previous studies (for example, see Refs. 11, 12, and 24) the rotor blade was assumed to have uniform structural and inertial properties along its span. However, because the introduction of the discrete devices in the root region will itself add significant amount of stiffness to the system, the flap bending, lag bending, and torsional stiffness of the root region (20% of the span and thought of as representing the "flexure") have been reduced to 70% of its baseline (see Table 1). The discrete devices are then introduced (attached at the intersection point between the softened inboard flexure and the outboard blade), and their spring constants adjusted such that the blade rotating natural frequencies are virtually identical to those of the uniform blade (without discrete devices). The tuned spring constants of the discrete devices as well as the resultant rotor frequencies are provided in Table 1, and it is this configuration, with the softened root element and discrete devices, that is considered as the baseline for this study. If the root element had not been softened to hold the rotor frequencies close to those of a typical soft-inplane hingeless rotor, the vibration reductions predicted would have applied to unrealistic rotor designs.

The introduction of discrete controllable stiffness devices near the blade root (a discrete flap spring, a lag spring, and a torsional spring, whose spring constants are not insignificant) raises questions about the required finite element discretization along the span and the number of modes required to effectively represent the system. Because it is possible that a finer finite element mesh may be required, especially in the root region, or a larger number of modes may be required in the modal transformation, a convergence study is first conducted in Sec. IV.B. Once the number of finite elements to model the blade and the number of modes required to represent the system with the discrete controllable stiffness devices have been established, hub vibration reductions caused by optimal cyclic stiffness variations of the discrete devices are examined in Sec. IV.C.

B. Convergence Study

1. *Number of Finite Elements Along the Blade Span*

A nominal number of five equal spanwise finite elements is used to capture the elastic flap bending, lag bending, and torsion deformations of the blade (Fig. 4a), with the discrete devices connected between the two innermost elements (at around 20% span). Variation in blade frequencies (up to 20/rev) and the corresponding mode shapes is examined when increasing numbers of spanwise elements are used (as shown in Figs. 4b–4d), with a finer concentration of elements near the root region where the discrete devices are attached. The variation in blade natural frequencies with increasing numbers of elements is shown in Fig. 5. From the figure it is seen that starting with a nominal five spanwise elements and going up to 19 spanwise elements results in virtually no change in the first 10 modal frequencies (up to 20/rev). Figures 6 and 7, respectively, show the flap and torsion mode shapes when increasing numbers of spanwise elements are used. From the figures it is seen that when an increasing number of elements is used the first four flap mode shapes and the first two torsion mode shapes show little variation. The first four lag modes displayed identical characteristics to the flap modes, and these results are therefore not presented. From the preceding results it is concluded that five spanwise finite elements (30 degrees of freedom – 10 flap bending, 10 lag bending, and 10 torsion) are sufficient to capture the lowest 10 modes (up to

Table 1 Rotor and fuselage properties

	Property	Value
Main rotor properties	Number of blades	4
	lock number γ	6.34
	Solidity ratio σ	0.1
	Rotational speed Ω	40.1234 rad/s
	C_T/σ	0.07
Rotor blade properties	Blade radius R	16.2 ft.
	Blade chord c/R	0.08
	Mass per unit length m_0	0.135 slug/ft
	Flap-bending stiffness $EI_\beta/M_0\Omega^2R^4$	0.008345
	Lag-bending stiffness $EI_\zeta/m_0\Omega^2R^4$	0.023198
	Torsional stiffness $GJ/m_0\Omega^2R^4$	0.003822
	Lift curve slope a	5.73
	Skin-friction drag coefficient C_{d0}	0.0095
	Induced drag coefficient C_{d2}	0.2
	Pitching moment coefficient C_m	0.0
Root element (flexure) properties	Flap-bending stiffness $EI_\beta^{\text{root}}/EI_\beta$	0.70
	Lag-bending stiffness $EI_\zeta^{\text{root}}/EI_\zeta$	0.70
	Torsional stiffness GJ^{root}/GJ	0.70
Controllable stiffness device properties	$\bar{K}_w/(EI_\beta/R^3)$	0.12231
	$\bar{K}_v/(EI_\zeta/R^3)$	0.11996
	$\bar{K}_\phi/(GJ/R^2)$	0.00716
	α_w, α_v	15°
	e_w, e_v	0.5c
Blade natural frequencies	Flap	1.147, 3.399, 7.447, 13.342/rev
	Lag	0.750, 4.364, 10.963, 20.653/rev
	Torsion	4.590, 13.595/rev
Tail rotor properties	Number of blades N_{tr}	4
	Tail rotor radius R_{tr}	3.24 ft.
	Solidity ratio σ_{tr}	0.15
	Rotor speed Ω_{tr}	5 Ω
	Lift curve slope a_{tr}	6.0
	Tail rotor location $(x_{\text{tr}}/R, z_{\text{tr}}/R)$	(1.2, 0.2)
Horizontal tail properties	Horizontal tail area $S_{\text{ht}}/\pi R^2$	0.011
	Horizontal tail lift curve slope a_{ht}	6.0
	Horizontal tail location x_{ht}/R	0.95
Rigid fuselage properties	c.g. location $(x_{\text{cg}}, y_{\text{cg}})$	(0, 0)
	Hub location h/R	0.2
	Net weight W	5800 lbs

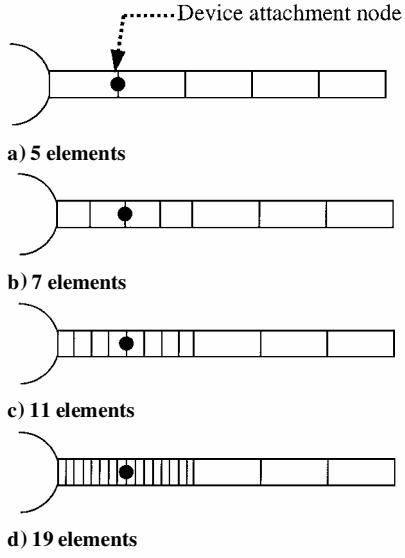

Fig. 4 Rotor blade finite element discretization used in the convergence study.

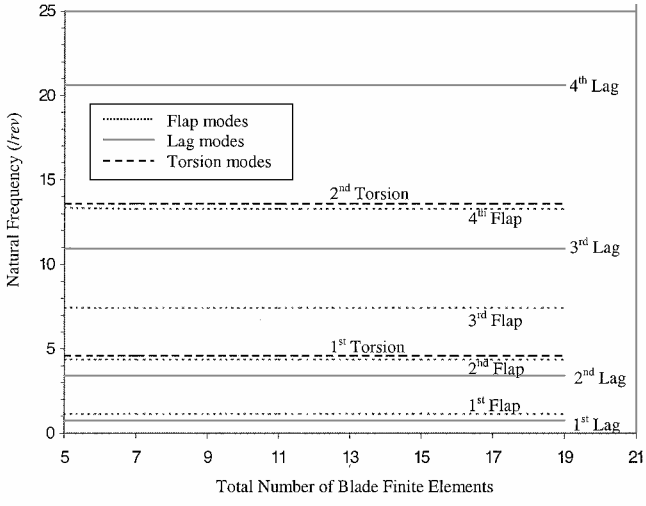

Fig. 5 Rotating system natural frequencies for increasing number of finite elements.

20/rev), and even in the presence of discrete stiffness devices in the blade root region increasing the number of elements does not improve accuracy of modal frequencies or mode shapes. Consequently, a total of five spanwise elements are used to model the blade hereafter.

2. Number of Blade Modes in Modal Transformation

In helicopter aeroelastic analyses it is common to transform the blade finite element equations of motion to a few modal equations to calculate the blade periodic response in forward flight in a computationally efficient manner. The number of modes used in the transformation, however, has to be sufficient to accurately capture the hub vibrations. In the present study even greater care is required because the discrete devices are cyclically changing their stiffness coefficients around the azimuth, and it is not known, a priori, how many modes would be required to predict the hub vibrations accurately. This section examines the effect of using increasing numbers of flap, lag, and torsion modes on the vibratory hub load predictions. Simulations are carried out at an advance ratio of 0.35, with one key simplification—the Drees (linear) inflow model is used rather than obtaining the inflow from the free wake, in calculating the blade sectional aerodynamic loads. Although it is recognized that this could lead to underprediction in hub vibration levels, the emphasis in this section is to establish the number of modes required to predict hub vibrations with cyclic stiffness variations of discrete devices, rather

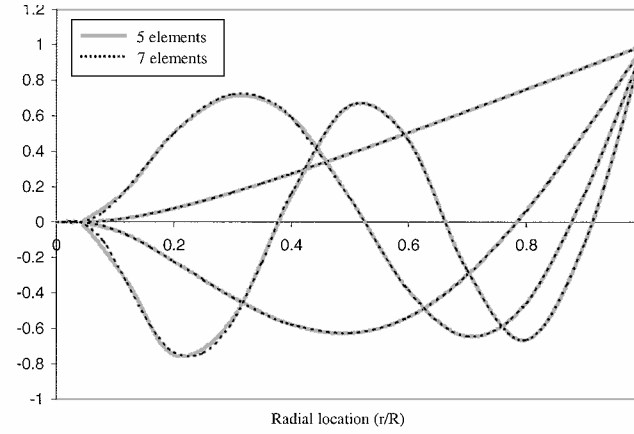

Fig. 6 Blade flap mode shapes for increasing number of finite elements.

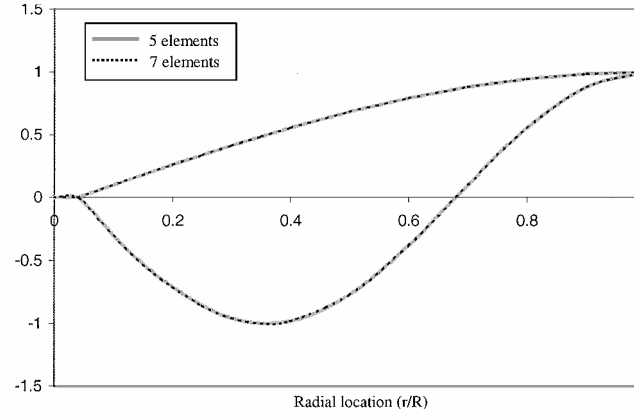

Fig. 7 Blade torsional mode shapes for increasing number of finite elements.

than predicting the "correct" vibration levels using a more sophisticated aerodynamic model.

Using, nominally, two flap, two lag, and two torsion modes (along with the Drees inflow model, at an advance ratio of 0.35), optimal 2/rev and 3/rev stiffness variations of the flap device, 2/rev and 3/rev stiffness variations of the lag device, and 3/rev and 4/rev stiffness variations of the torsion device were first determined (see Table A1 in the Appendix). The baseline vibration levels (no cyclic stiffness variations) and the reduced vibration levels obtained when using the flap device, lag device, or torsion device (with inputs in Table A1) were also recorded (see Table A2). Next, for the optimal 2/rev and 3/rev stiffness variations of the flap device the hub vibration levels were calculated using increasing number of flap modes. (Inputs were held constant, not recalculated for increasing number of modes.) These results are shown in Fig. 8. The figure clearly indicates that for a given optimal cyclic stiffness variation of the flap device when the number of flap modes is greater than four no change in any component of the predicted 4/rev vibratory hub loads is observed. This process was then repeated using optimal stiffness variations of the lag device and progressively increasing the number of lag modes, and using optimal stiffness variations of the torsion device and progressively increasing the number of torsion modes—and for both cases, examining the effects of increasing number of modes on predicted 4/rev hub vibrations. (Results not included.) The conclusion of this modal convergence study was that four flap modes, four lag modes, and two torsion modes were required to predict the 4/rev hub vibration levels, when the stiffness of the discrete devices is cyclically varied around the azimuth. These are the number of modes used in the vibration reduction studies in Sec. IV.C.

C. Hub Vibration Reductions Using Controllable Stiffness Devices

The effectiveness of optimal multi-cyclic variations in the stiffness of the discrete devices, on reducing the 4/rev hub vibration

Table 2a 4/rev vibratory hub loads for baseline rotor—no cyclic stiffness variation (free wake, $\mu = 0.3$)

4/rev vibratory hub loads	Values
F_x [a]	1.171942
F_y [b]	2.241857
F_z [c]	2.635219
M_x [d]	37.758708
M_y [e]	40.251373
M_z [f]	54.868240

[a] F_x = drag force.
[b] F_y = side force.
[c] F_z = vertical force.
[d] M_x = rolling moment.
[e] M_y = pitching moment.
[f] M_z = yawing moment. [All forces are % of F_z^0 (5914 lbs). All moments are % of M_z^0 (4878 ft-lbs).]

Table 2b Harmonics of blade root loads for baseline rotor—no cyclic stiffness variation (free wake, $\mu = 0.3$)

Blade root loads	Harmonics				
	1/rev	2/rev	3/rev	4/rev	5/rev
S_r [a]	16.5412	1.793	0.348	1.5112	0.2833
S_x [b]	13.5271	0.8518	0.9605	3.4555	0.5395
S_z [c]	4.3921	1.3569	5.9717	0.6584	0.4924
M_ϕ [d]	−1.624	−0.53	−0.175	−0.256	−0.031
M_β [e]	−20.017	−4.484	−19.397	−1.991	−1.421
M_ζ [f]	−77.574	−3.881	−3.617	−13.745	−1.96

[a] S_r = radial shear.
[b] S_x = drag shear.
[c] S_z = vertical shear.
[d] M_ϕ = pitching moment.
[e] M_β = flap moment.
[f] M_ζ = lag moment. [All forces are % of $M_0 r^2 R^2$. All moments are % of $M_0 r^2 R^3$.]

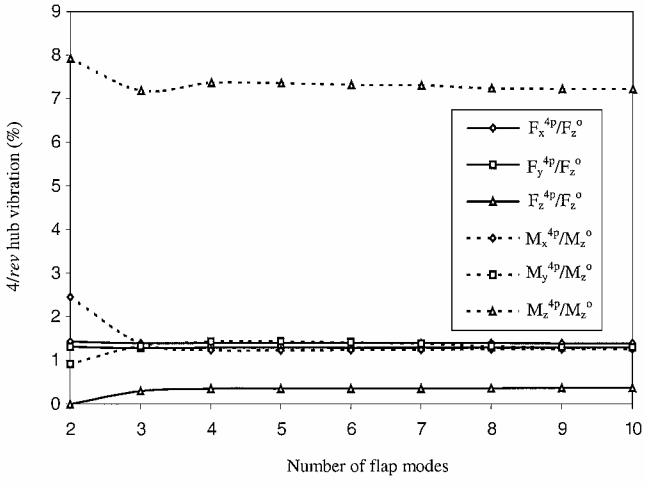

Fig. 8 Variation in 4/rev vibratory hub load predictions with increasing number of flap modes, when a 2,3/rev flap stiffness variation is used (Drees inflow, $\mu = 0.35$).

levels, is examined in this section. The 4/rev hub vibrations for the baseline helicopter, in the absence of any cyclic stiffness variation, are first obtained at an advance ratio of 0.3, with the inclusion of a full free wake in the calculation of the blade sectional aerodynamic loads. These results are given in Table 2a, and the corresponding vibratory blade root loads (first through fifth harmonics) are given in Table 2b. The hub vibration levels in Table 2a correspond to a vibration performance index $J_z = 100$ and are used as point of reference to which vibration levels are compared when optimal multi-cyclic stiffness variations are introduced. Sections IV.C.1–IV.C.3 examine the vibration reductions obtained when multi-cyclic stiffness variations of a flap device, a lag device, and

Table 3 Optimal 2,3/rev flap device stiffness variations ($J_z = 69.25$)

Input	Amplitude ($\Delta K_w/\bar{K}_w$), %	Phase, deg
2/rev	18.4	44.4
3/rev	47.1	140.8

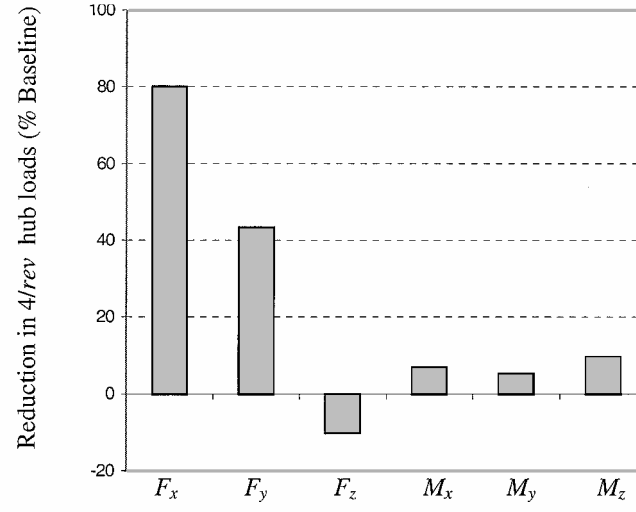

Fig. 9 Hub vibration reduction caused by optimal 2,3/rev flap device stiffness variations.

a torsion device are considered individually. Only 2/rev and 3/rev stiffness variations of the discrete flap and lag devices and 3/rev and 4/rev stiffness variations of the discrete torsion device are considered because previous studies showed that these components had the greatest influence on hub vibrations.[11,12] Based on the vibration reductions obtained with the individual devices, Sec. IV.C.4 evaluates the reductions possible when optimal multi-cyclic stiffness variations of the flap and lag devices are simultaneously considered. Finally, Sec. IV.C.5 and IV.C.6 demonstrate the effectiveness of the discrete controllable stiffness devices in reducing hub vibration levels for variations in configuration properties and cruise speed, respectively.

1. *Optimal 2,3/rev Flap Device Stiffness Variations*

Multi-cyclic variations in the spring coefficient of only the flap stiffness device (see Fig. 1a and the mathematical representation in Fig. 1b) are considered first. The optimal 2/rev and 3/rev flap stiffness variations (amplitude and phase values) are determined using the approach described in Sec. III and are presented in Table 3. For these optimal stiffness variations the output vibration index J_z is reduced by 31%, compared to the baseline value. The corresponding reductions in individual components of vibratory hub loads are shown in Fig. 9. An 80% reduction in in-plane hub drag force F_x^{4p} and a 45% reduction in in-plane hub side force F_y^{4p} are observed. Changes in the other components of vibratory hub loads are less than 10%. The variation in device stiffness over a single rotor revolution is shown in Fig. 10 and is bounded between 35 and 160% of the baseline value $\bar{K}_w$.

2. *Optimal 2,3/rev Lag Device Stiffness Variations*

Next, multi-cyclic variations in the spring coefficient of the lag stiffness device (see Fig. 1a and the mathematical representation in Fig. 1c) are considered. The optimal 2/rev and 3/rev stiffness variations of the lag device are presented in Table 4. These optimal lag device stiffness variations result in a 16% reduction in the vibration index J_z relative to the baseline, with changes in the individual components of vibratory hub loads shown in Fig. 11. From the figure a 45% reduction in in-plane hub drag force F_x^{4p} and a 25% reduction in in-plane hub side force F_y^{4p} are observed, with the

Table 4 Optimal 2,3/rev lag device stiffness variations (J_z = 84.23)

Input	Amplitude ($\Delta K_v/\bar{K}_v$), %	Phase, deg
2/rev	36.8	33.4
3/rev	14.3	−160.3

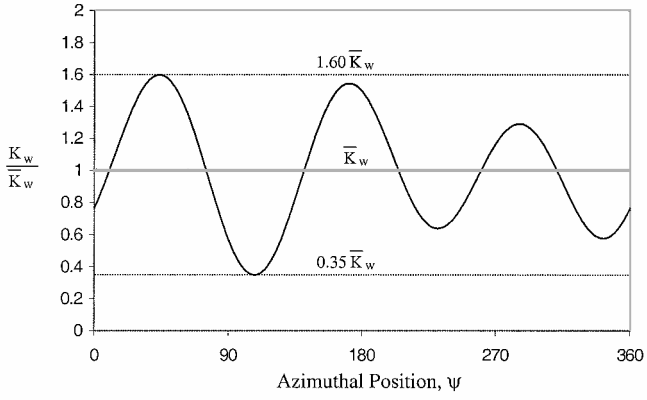

Fig. 10 Time history of optimal 2,3/rev flap device stiffness variations, presented in Table 3.

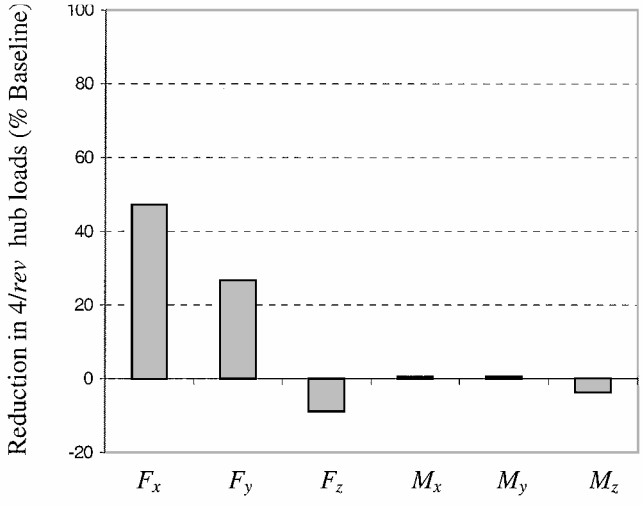

Fig. 11 Hub vibration reduction caused by optimal 2,3/rev lag device stiffness variations.

other components not showing any significant changes. The combination of the 2/rev and 3/rev inputs (amplitude and phase) implies that the lag device stiffness varies between 53 and 150% of the baseline value $\bar{K}_v$ over a single rotor revolution (stiffness variation not shown).

3. *Optimal 3,4/rev Torsion Device Stiffness Variations*

Multi-cyclic variations in the spring coefficient of the controllable torsion stiffness device are considered next (see Fig. 1a and the mathematical representation in Fig. 1d). Optimal 3/rev and 4/rev torsion stiffness variations are presented in Table 5a and the corresponding reductions in individual components of vibratory hub loads are shown in Fig. 12. Only a very modest reduction (under 5%) in the vibratory vertical hub force F_z^{4p} is observed, and other components of hub vibratory loads have even lower sensitivity. These observations are qualitatively similar to those previously reported,[11] but the percentage reduction in F_z^{4p} is even smaller as a result of the higher baseline vibration levels associated with the inclusion of the free wake in the present analysis. For the results in Table 5a and Fig. 12,

Table 5a W_k = 0.020[I], baseline torsion device stiffness = $\bar{K}_\phi$

Input	Amplitude ($\Delta K_\phi/\bar{K}_\phi$), %	Phase, deg
3/rev	18.7	−176.1
4/rev	46.8	151.9

Table 5b W_k = 0.015[I], baseline torsion device stiffness = $\bar{K}_\phi$

Input	Amplitude ($\Delta K_\phi/\bar{K}_\phi$), %	Phase, deg
3/rev	25.1	−179.3
4/rev	60.8	152.5

Table 5c W_k = 0.015[I], baseline torsion device stiffness = 2 $\bar{K}_\phi$

Input	Amplitude ($\Delta K_\phi/2\bar{K}_\phi$), %	Phase, deg
3/rev	25.2	−175.5
4/rev	59.7	166.4

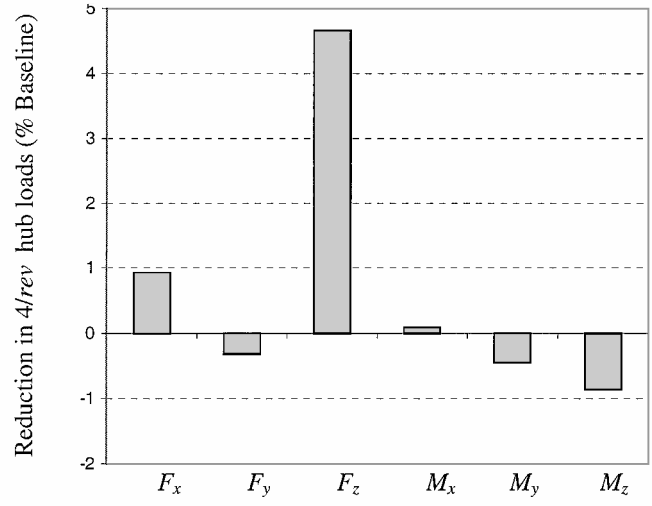

Fig. 12 Hub vibration reduction caused by optimal 3,4/rev torsion device stiffness variations (W_k = 0.02[I], baseline torsion device stiffness = $\bar{K}_\phi$).

a penalty weighting on the input of $W_k = 0.02I$ was used, as the default value of $W_k = I$ (for results in Sec. IV.C.1 and IV. C .2) produced torsion stiffness variations that were very small and no negligible change in vibratory hub loads.

To examine whether any further reductions in hub vibration were possible using cyclic torsion stiffness variations, two additional cases are considered. In the first case the penalty weighting W_k is reduced (from $0.02I$ to $0.015I$), allowing for larger percentage variations in spring coefficient. In the second case, recognizing that the arbitrarily large percentage changes in spring coefficient are not permissible and yet it is the actual physical values of the stiffness changes that matter, $\bar{K}_\phi$ is itself increased to twice the baseline value. In this case larger torsion stiffness variation can be introduced even while the change in spring coefficient, as a percentage of the baseline, is kept bounded. (Of course, the baseline rotor frequencies and vibration characteristics themselves undergo some change.) The reductions in the vibratory vertical hub force F_z^{4p} for these two cases, shown in Fig. 13, suggest that only small improvements are possible. The corresponding optimal stiffness variations are given in Tables 5b and 5c. Because multi-cyclic torsion stiffness variations are clearly much less influential than flap and lag stiffness variations, they are not further considered for semi-active helicopter vibration reduction.

Table 6 Optimal 2,3/rev flap and lag devices stiffness variations (J_z = 67.23)

Input		Amplitude	Phase, deg
Flap device	2/rev	$\Delta K_w = 5.5\% \bar{K}_w$	30.1
stiffness variation	3/rev	$\Delta K_w = 43.5\% \bar{K}_w$	139.7
Lag device	2/rev	$\Delta K_v = 32.2\% \bar{K}_v$	59.7
stiffness variation	3/rev	$\Delta K_v = 8.9\% \bar{K}_v$	109.4

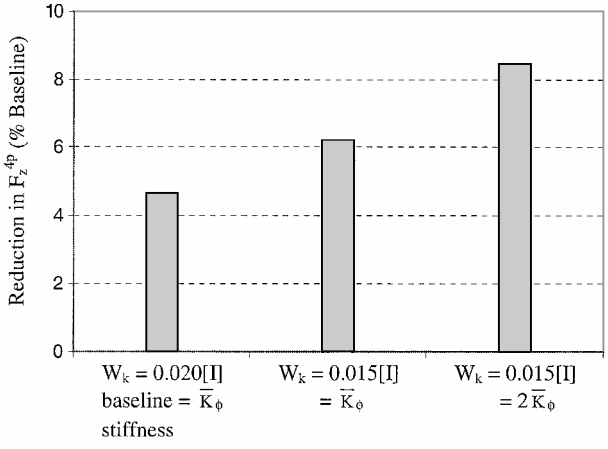

Fig. 13 Hub vibration reduction caused by the optimal 3,4/rev torsion device stiffness variations with varying input weights (W_k) and baseline torsion spring stiffness ($\bar{K}_\phi$, $2\bar{K}_\phi$).

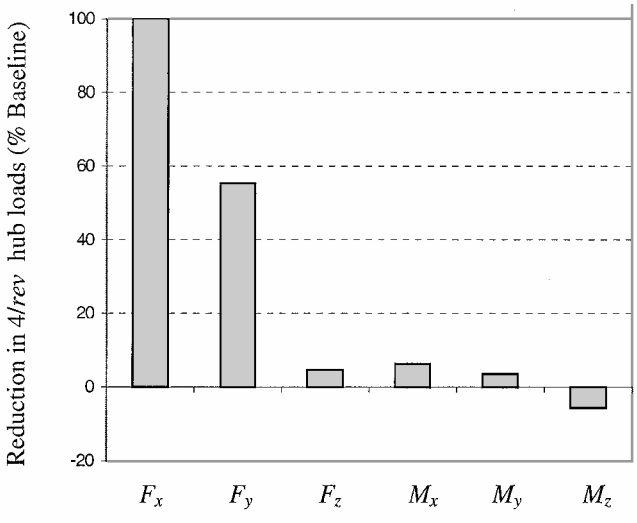

Fig. 14 Hub vibration reduction caused by optimal 2,3/rev flap and lag device stiffness variations.

4. Optimal 2,3/rev Flap and Lag Device Stiffness Variations

From the results in Sec. IV.C.1–IV.C.3, it is clearly established that multi-cyclic variations in either flap or lag device stiffness can significantly reduce some components of hub vibration, but variation in torsion stiffness is relatively ineffective. The present section examines the possible reductions in vibratory hub loads when optimal 2/rev and 3rev flap and 2/rev and 3rev lag stiffness variations are simultaneously considered. (These results are presented in Fig. 14, and the corresponding optimal inputs are shown in Table 6.) The optimal stiffness variations produce a 33% reduction in vibration index. It is seen that vibratory in-plane hub drag force F_x^{4p} is virtually eliminated, and the hub side force F_y^{4p} is reduced by 55%. Only minor changes in other components of hub loads are observed.

For the optimal flap and lag stiffness variations Table 7 shows the percentage changes in the first through fifth harmonics of the various components of blade root loads (with reference to the baseline values given in Table 2b). None of the components of blade root loads show any significant increases. The third through fifth harmonics of the

Table 7 Percentage change in harmonics of blade root loads caused by the optimal 2,3/rev flap and lag device stiffness variations

Blade root loads	Percentage change in harmonics				
	1/rev	2/rev	3/rev	4/rev	5/rev
S_r	−0.34	−4.20	9.46	10.27	5.03
S_x	−0.47	−8.23	−40.02	8.23	−0.14
S_z	−0.61	3.32	−23.42	−4.79	−10.87
M_ϕ	−0.36	−1.26	7.10	12.03	9.61
M_β	−0.32	0.67	−4.53	−14.70	−23.13
M_ζ	−0.83	−28.53	−11.18	5.60	0.30

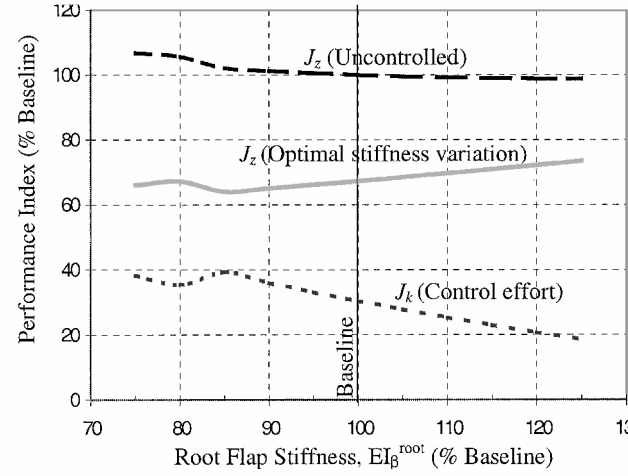

Fig. 15 Effectiveness of optimal 2,3/rev flap and lag device stiffness variations for changes in root element (flexure) flap stiffness.

blade root radial shear S_r show increases between 5–10%; the fourth harmonic of the blade root drag shear S_x shows an 8% increase; the third through fifth harmonics of the blade root pitching moment M_ϕ show between 7–12% increases; and the fourth harmonic of the blade root lag moment M_ζ shows a 5% increase. Significant reductions seen were in the third harmonic of S_x (40%), second harmonic of M_ζ (30%), third harmonic of the blade root vertical shear S_z (23%), and fifth harmonic of the blade root flapping moment M_β (40%).

5. Vibration Reduction for Changes in System Properties (Root Element Flexural Stiffness)

In Sec. IV.C.4 simultaneous multi-cyclic variations in spring coefficients of both the flap and lag devices were seen to significantly reduce the hub vibration levels of the baseline configuration whose properties are given in Table 1. The present section verifies that the concept of using multi-cyclic variations in spring coefficients of discrete controllable stiffness devices would be effective even if the baseline configuration changes. Keeping the discrete controllable devices unchanged from the baseline, the flap, lag, and torsion stiffness of the blade root element (representative of the flexure) is individually varied by ±25% of its nominal value. The optimal 2,3/rev flap and lag device stiffness variations are reevaluated, and their influence examined on the vibratory hub loads. Figures 15–17 show reductions in vibration index J_z for variations in flap, lag, and torsion stiffness of the flexure, respectively. Overall, the multi-cyclic controller retains its effectiveness (producing 25–35% reduction in vibration index J_z compared to the uncontrolled case) over the range of variations considered in the flap, lag, and torsion stiffness of the flexural element. The control effort index J_k shows a slight increase when the flap stiffness or lag stiffness of the flexural element is reduced.

6. Effectiveness of Vibration Controller at Different Forward Speeds

This section examines the effectiveness of 2/rev and 3/rev flap and lag stiffness variations for vibration reduction at different cruise

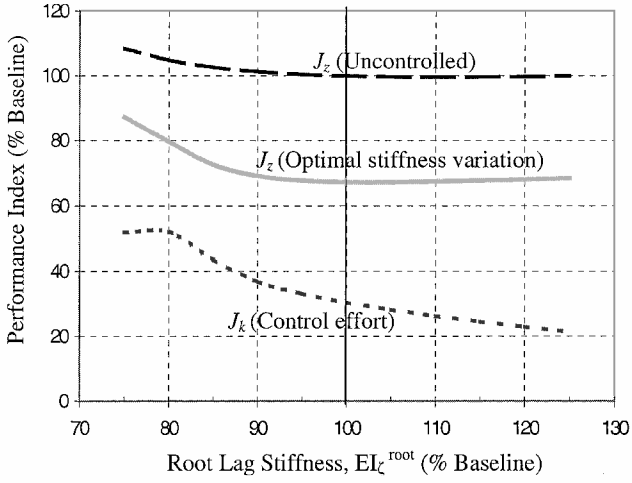

Fig. 16 Effectiveness of optimal 2,3/rev flap and lag device stiffness variations for changes in root element (flexure) lag stiffness.

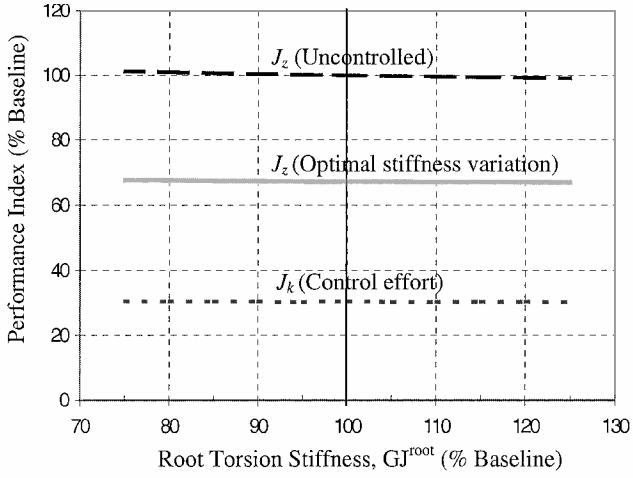

Fig. 17 Effectiveness of optimal 2,3/rev flap and lag device stiffness variations for changes in root element (flexure) torsion stiffness.

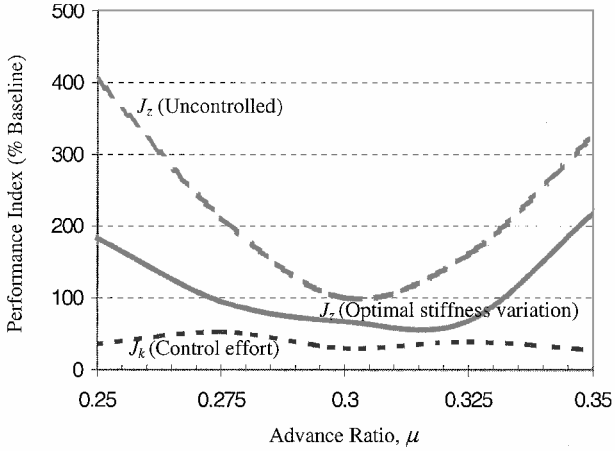

Fig. 18 Effectiveness of optimal 2,3/rev flap and lag device stiffness variations for different advance ratios.

speeds. Figure 18 shows the vibration performance index J_z with and without the multi-cyclic stiffness variations over forward speed ranging from advance ratio of 0.25 to 0.35 (the optimal stiffness variations are recalculated at different flight speeds). The vibration performance index is normalized with respect to the baseline (uncontrolled) vibrations at an advance ratio of 0.30 given in Table 2a (corresponding to $J_z = 100$). It is seen that as the advance ratio increases from 0.30 to 0.35, the uncontrolled vibration index increases from 100 to 320. As the advance ratio decreases from 0.30 to 0.25, the uncontrolled vibration index again increases from 100 to 400, as a result of the dominant effect of the rotor wake at the lower advance ratio. With optimal 2/rev and 3/rev stiffness variations of the flap and lag devices, the vibration index shows reductions across the advance ratio range. The reductions in J_z, relative to the uncontrolled case, vary from 55% at an advance ratio of 0.25 to around 33% at advance ratios between 0.3 and 0.35. The control effort index J_k shows only mild variations over the range of forward speeds considered, despite the large differences in the uncontrolled vibration levels.

V. Conclusions

In the present study it is demonstrated that cyclically varying the stiffness of discrete controllable stiffness devices introduced in the blade root region produces reductions in the 4/rev vibratory hub loads of a four-bladed hingeless rotor helicopter. The controllable stiffness devices (a flap stiffness device, a lag stiffness device, and a torsion stiffness device) are modeled as discrete springs whose stiffness coefficients can be varied, and their influence is included in a comprehensive rotorcraft aeroelastic analysis. Finite element and modal convergence studies were conducted to ensure accuracy of hub vibration predictions in the presence of the discrete springs with cyclically varying stiffness. A gradient-based optimization scheme is used to determine the optimal multi-cyclic stiffness variation inputs that minimize a composite vibration index (comprising of all six components of vibratory hub loads). Devices introduced to cyclically control the flap and lag stiffness of the rotor were effective in substantially reducing the in-plane 4/rev vibratory hub forces. When optimal 2/rev and 3/rev flap and lag device stiffness variations were used in combination, the vibratory hub drag force was practically eliminated, and the vibratory hub side force was reduced by 55%. No significant detrimental effects were observed on the first through the fifth harmonics of the vibratory blade root loads. Multi-cyclic stiffness variations of the torsion device produced only small reductions in the 4/rev hub vertical force. Multi-cyclic stiffness variations of the flap and lag devices were seen to be effective in reducing hub vibration even when the fundamental rotor properties such as the flap, lag, and torsion stiffness of the root (flexure) element, and the operating condition (forward speed) were changed.

Appendix: Convergence Study

Table A1 Optimal stiffness variations predicted using two flap, two lag, and two torsion modes (Drees inflow, $\mu = 0.35$)

Input		Amplitude	Phase, deg
Flap device	2/rev	$\Delta K_w = 29.3\% \bar{K}_w$	143.6
stiffness variation	3/rev	$\Delta K_w = 68.3\% \bar{K}_w$	36.9
Lag device	2/rev	$\Delta K_v = 25.1\% \bar{K}_v$	−74.4
stiffness variation	3/rev	$\Delta K_v = 49.8\% \bar{K}_v$	−167.1
Torsion device	3/rev	$\Delta K_\phi = 48.1\% \bar{K}_\phi$	−8.3
stiffness variation	4/rev	$\Delta K_\phi = 42.0\% \bar{K}_\phi$	134.9

Table A2 4/rev vibratory hub loads (predicted using two flap, two lag, and two torsion modes) with and without stiffness variations (Drees inflow, $\mu = 0.35$)

4/rev hub loads	Baseline values	With 2,3/rev flap stiffness variation	With 2,3/rev lag stiffness variation	With 3,4/rev torsion stiffness variation
F_x[a]	2.06	1.43	1.79	2.07
F_y[b]	2.08	1.31	1.65	2.07
F_z[c]	1.23	0.002	0.12	1.13
M_x[d]	10.52	2.46	10.33	10.42
M_y[e]	11.26	0.91	10.41	11.00
M_z[f]	10.52	7.92	12.34	9.78

[a] F_x = drag force.
[b] F_y = side force.
[c] F_z = vertical force.
[d] M_x = rolling moment.
[e] M_y = pitching moment.
[f] M_z = yawing moment. [All forces are % of F_z^0 (6042 lbs). All moments are % of M_z^0 (6556 ft-lbs).]

References

[1]Reichert, G., "Helicopter Vibration Control-Survey," *Vertica*, Vol. 5, No. 1, 1981, pp. 1–20.

[2]Lowey, R. G., "Helicopter Vibrations: A Technological Perspective," *Journal of the American Helicopter Society*, Vol. 29, No. 4, 1984, pp. 4–30.

[3]Nguyen, K., "Higher Harmonic Control Analysis for Vibration Reduction of Helicopter Rotor Systems," Ph.D. Dissertation, Dept. of Aerospace Engineering, Univ. of Maryland, College Park, 1989.

[4]Milgram, J. H., and Chopra, I., "A Parametric Design Study for Actively Controlled Trailing Edge Flaps," *Journal of the American Helicopter Society*, Vol. 43, No. 2, 1998, pp. 110–119.

[5]Welsh, W., Fredrickson, C., Rauch, C., and Lyndon, I., "Flight Test of An Active Vibration Control System on the UH-60 Black Hawk Helicopter," *Proceedings of the American Helicopter Society 51st Annual Forum*, Vol. 1, American Helicopter Society, Alexandria, VA, May 1995, pp. 393–402.

[6]Staple, A. E., "An Evaluation of Active Control of Structural Response as a Means of Reducing Helicopter Vibration," *Proceedings of the American Helicopter Society 46th Annual Forum*, Vol. 1, American Helicopter Society, Alexandria, VA, May 1990, pp. 3–17.

[7]Ganguli, R., and Chopra, I., "Aeroelastic Optimization of an Advanced Geometry Helicopter Rotor," *Journal of the American Helicopter Society,* Vol. 41, No. 1, 1996, pp. 18–28.

[8]Chen, P., and Chopra, I., "Induced Strain Actuation of Composite Beams and Rotor Blades with Embedded Piezoceramic Elements," *Proceedings of the Society of Photo-Optical Instrumentation Engineers on Smart Structures and Materials*, SPIE, Vol. 2190, Society of Photo-Optical Instrumentation Engineers, Bellingham, WA, 1994, pp. 123–140.

[9]Jacklin, S. A., Blaas, A., Teves, D., and Kube, R., "Reduction of Helicopter BVI Noise, Vibration and Power Consumption Through Individual Blade Control," *Proceedings of the American Helicopter Society 51st Annual Forum*, Vol. 1, American Helicopter Society, Alexandria, VA, May 1995, pp. 662–680.

[10]Shaw, J., Albion, N., Hanker, E. J., Jr., and Teal, R. S., "Higher Harmonic Control: Wind Tunnel Demonstration of Fully Effective Vibratory Hub Force Suppression," *Journal of the American Helicopter Society,* Vol. 34, No. 1, 1989.

[11]Anusonthi-Inthra, P., and Gandhi, F., "Helicopter Vibration Reduction through Cyclic Variations in Rotor Blade Root Stiffness," *Journal of Intelligent Material Systems and Structures*, Vol. 11, No. 2, 2000, pp. 153–166.

[12]Anusonti-Inthra, P., and Gandhi, F., "Optimal Control of Helicopter Vibration Through Cyclic Variations in Blade Root Stiffness," *Smart Materials and Structures*, Vol. 10, No. 1, 2001, pp. 86–95.

[13]Yang, J. N., Wu, J. C., and Li, Z., "Control of Seismic-Excited Buildings Using Active Variable Stiffness Systems," *Engineering Structures,* Vol. 19, No. 9, 1996, pp. 589–596.

[14]Patten, W. N., Mo, C., Kuehn, J., and Lee, J., "A Primer on Design of Semiactive Vibration Absorbers (SAVA)," *Journal of Engineering Mechanics*, Vol. 124, No. 1, 1998, pp. 61–68.

[15]Sadek, F., and Mohraz, B., " Semiactive Control Algorithms for Structures with Variable Dampers," *Journal of Engineering Mechanics*, Vol. 124, No. 9, 1998, pp. 981–990.

[16]Gavin, H. P., and Doke, N. S., "Resonance Suppression Through Variable Stiffness and Damping Mechanisms," *Proceedings of the SPIE Smart Structures Conference*, SPIE, Vol. 3671, Society of Photo-Optical Instrumentation Engineers, Bellingham, WA, March 1999, pp. 43–53.

[17]Krasnicki, E. J., "Comparison of Analytical and Experimental Results for a Semi-Active Vibration Isolator," *The Shock and Vibration Bulletin*, The Shock and Vibration Information Center, Naval Research Lab., Washington, DC, Vol. 50, Pt. 4, 1980, pp. 69–76.

[18]Krasnicki, E. J., " The Experimental Performance of an Off-Road Vehicle Utilizing a Semi-Active Suspension," *The Shock and Vibration Bulletin,* The Shock and Vibration Information Center, Naval Research Lab., Washington, DC, Vol. 54, Pt. 3, 1984, pp. 135–142.

[19]Hrovat, D., Margolis, D. L., and Hubbard, M., "An Approach Toward the Optimal Semi-Active Suspension," *Journal of Dynamic Systems, Measurement, and Control*, Vol. 110, No. 3, 1988, pp. 288–296.

[20]Karnopp, D., "Design Principles for Vibration Control Using Semi-Active Dampers," *Journal of Dynamic Systems, Measurement, and Control*, Vol. 112, No. 3, 1990, pp. 448–455.

[21]Symans, M. D., and Constantinou, M. C., "Semi-Active Control Systems for Seismic Protection of Structures: A State-of-the-Art Review," *Engineering Structures*, Vol. 21, 1999, pp. 469–487.

[22]Marathe, S., Gandhi, F., and Wang, K. W., "Helicopter Blade Response and Aeromechanical Stability with a Magnetorheological Fluid Based Lag Damper," *Journal of Intelligent Material Systems and Structures*, Vol. 9, No. 4, 1998, pp. 272–282.

[23]Kamath, G. M., Wereley, N. M., and Jolly, M. R., "Characterization of Magnetorheological Helicopter Lag Dampers," *Journal of the American Helicopter Society*, Vol. 44, No. 3, 1999, pp. 234–248.

[24]Bir, G., and Chopra, I., "University of Maryland Advanced Rotorcraft Code (UMARC) Theory Manual," Univ. of Maryland, UM-AERO Rept. 92-02, College Park, MD, Aug. 1992.

[25]Tauszig, L., "Numerical Detection and Characterization of Blade-Vortex Interactions Using a Free Wake Analysis," M.S. Thesis, Dept. of Aerospace Engineering, Pennsylvania State Univ., University Park, PA, Aug. 1998.

[26]Gandhi, F., and Tauszig, L., "A Critical Evaluation of Various Approaches for the Numerical Detection of Helicopter Blade-Vortex Interactions," *Journal of the American Helicopter Society*, Vol. 45, No. 3, 2000, pp. 179–190.

[27]Johnson, W., "Self-Tuning Regulators for Multicyclic Control of Helicopter Vibration," NASA TP 1996, March 1982.